Relation of the Second Type Thermal Helicity to Precipitation of Landfalling Typhoons: A Case Study of Typhoon Talim*

YU Zifeng†(喻自凤) and YU Hui(余 晖)

Shanghai Typhoon Institute/Laboratory of Typhoon Forecast Technique, CMA, Shanghai 200030

(Received June 21, 2010)

ABSTRACT

This study utilized the MM5 mesoscale model to simulate the landfalling process of Typhoon Talim. The simulated typhoon track, weather patterns, and rainfall process are consistent with the observation. Using the simulation results, the relation of the second type thermal helicity (H_2) to rainfall caused by the landfalling typhoon Talim was analyzed. The results show that H_2 could well indicate the heavy inland rainfall but it did not perform as well as the helicity in predicting rainfall during the beginning stage of the typhoon landfall. In particular, H_2 was highly correlated with rainfall of Talim at 1-h lead time. For 1–5-h lead time, it also had a higher correlation with rainfall than the helicity did, and thus showing a better potential in forecasting rainfall intensification. Further analyses have shown that when Talim was in the beginning stage of landfall, 1) the 850–200-hPa vertical wind shear around the Talim center was quite small (about 5 m s^{-1}); 2) the highest rainfall was to the right of the Talim track and in the area with a 300-km radius around the Talim center, exhibiting no obvious relation to low-level temperature advection, low-level air convergence, and upper-level divergence; 3) the low-level relative vorticity reflected the rainfall change quite well, which was the main reason why helicity had a better performance than H_2 in this period. However, after Talim moved inland further, 1) it weakened gradually and was increasingly affected by the northern trough; 2) the vertical wind shear was enhanced as well; 3) the left side of the down vertical wind shear lay in the Lushan and Dabieshan mountain area, which could have contributed to triggering a secondary vertical circulation, helping to produce the heavy rainfall over there; hence, H_2 showed a better capacity to reflect the rainfall change during this stage.

Key words: second type thermal helicity, typhoon, rainfall diagnosis

Citation: Yu Zifeng and Yu Hui, 2011: Relation of the second type thermal helicity to precipitation of landfalling typhoons: A case study of Typhoon Talim. *Acta Meteor. Sinica*, **25**(2), 224–237, doi: 10.1007/s13351-011-0029-4.

1. Introduction

Landfalling typhoons often bring heavy rainfall and even disasters. This has been a general consensus. Based on the statistical data in 1970–1999, it is found that the vast majority of deaths related to tropical cyclones in the United States resulted from inland flooding (Rappaport, 2000). In China, disasters caused by typhoons each year are also mainly related to heavy rainfall from typhoons. For example, the “75.8” flood caused by the typhoon No. 7503 resulted in losses of more than ten thousand human lives (Chen, 1977). Typhoon Bilis (2006) caused very heavy rainfall in Fujian, Guangdong, Jiangxi, Hunan, and Guangxi provinces, which led to 645 deaths (tropical cyclone annual report in 2006). Therefore, improving typhoon rainfall forecast is a key issue in typhoon research.

The nowcasting of typhoon rainfall is developed based on radar and satellite observations, but the validity time is quite limited. After the genesis of a typhoon over the tropical sea surface, the typhoon would experience extratropical transition during its motion toward the subtropics or during its landfall (Lei and Chen, 2001; Niu et al., 2005). Land use conditions, topography, and mesoscale vortices within the typhoon might influence typhoon precipitation distribution as well. It is rather difficult to quantitatively forecast

*Supported by the “973” Program of China (2009CB421505), National Natural Science Foundation of China (40405012, 40830958, 40705024, and 40875039), and Shanghai Meteorological Bureau (2009ST11).

†Corresponding author: yuzf@mail.typhoon.gov.cn.

(Chinese version published in Vol. 67, No. 5, 851–863, 2009)

typhoon rainfall. Marks and Shay (1998) pointed out that in order to improve the skill of quantitative precipitation forecast (QPF), it is necessary to investigate the vertical wind shear effects on the typhoon precipitation and to understand the physical mechanisms of rainfall process (including rain intensity and distribution). Diagnosis of physical quantities is one of the useful ways to forecast rainfall. So far, quantitative precipitation estimation (Pfost, 2000; Kidder et al., 2005; Cheung et al., 2006) and numerical model forecasting are principal methods used in predicting landfalling typhoon precipitation. Due to the limitation of computer resources, application of high-resolution numerical weather forecast models is still restricted in real-time operation. Thus, the diagnostic forecast based on the numerical weather forecast of rainfall models plays an important role, and this also helps to better understand physical process of rainfall.

Common physical quantities used in rainfall diagnosis include helicity, moist potential vorticity, relative vorticity, etc., which reflect effects of the horizontal circulations of vortices (Moffatt, 1969; Gao et al., 2004a, b, 2005; Gao, 2007; Zhao et al., 2009). Yu and Wang (2005) proposed the second type thermal helicity (H_2), which reflects the interaction between wind vectors and the horizontal vorticity tube caused by vertical wind shear. Du et al. (2007) used H_2 to analyze a heavy rainfall event in Shanghai during 5–6 August 2001, and found that H_2 performed well in the rainfall diagnosis.

Typhoon Talim landing in Hualian city of Taiwan at 0600 BT (Beijing Time) 1 September 2005 moved northwestward (Fig. 1) and landed in Putian area of Fujian Province again at 1430 BT on the same day. During the landfalling process, Talim brought torrential rains in some mountain areas such as Wuyi, Lushan, and Dabieshan. The torrential rainfalls lasted over 72 h and the total rainfall amount reached more than 940 mm, which resulted in direct economic loss of 15.46 billion yuans. This is a typical case of heavy rain disasters caused by a landfalling typhoon. In this study, we use H_2 to diagnose this rainfall process and to examine the diagnostic ability of H_2 during different

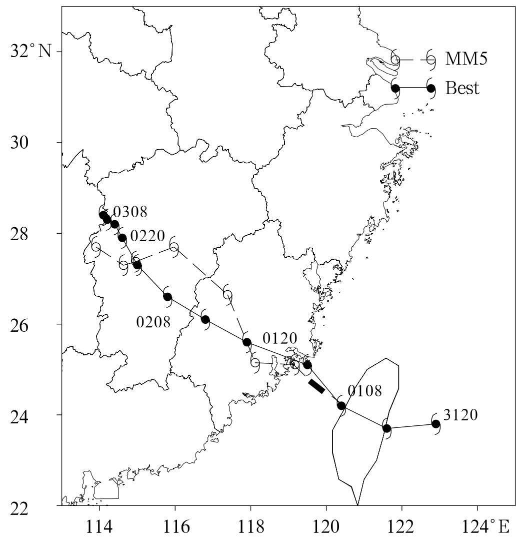

Fig. 1. Observed and simulated tracks of Typhoon Talim from 2000 BT 31 August to 1400 BT 3 September 2005. Number 3120 represents 2000 BT 31 August. Denotion of other numbers in the same form can be deduced. "Best" represents the observed track and "MM5" represents the MM5 simulated track.

landfall periods. The possible physical mechanisms that have sustained the rainfall process of Talim will be explored as well.

This paper is arranged as follows. Section 2 describes the configuration, integration, and verification of the fifth-generation NCAR/PSU Mesoscale Model (MM5). The diagnostic analysis of rainfall with H_2 during different landfall periods and the comparison with that using the classical helicity are provided in Section 3. The thermal and dynamical mechanisms of the heavy rainfall are analyzed in Section 4. Results are summarized in Section 5.

2. Model simulation and verification

2.1 Model configuration

In this study, the MM5 version 3.6 (Dudhia et al., 2001) is utilized in numerical simulations of the heavy rainfall event. The model domain covers an outer grid at a 27-km resolution with 101×101 (D01) mesh points, and an inner grid at a 9-km resolution with 181×181 (D02) mesh points. The domain center is at 30.0°N, 116.0°E. All grids have 30 levels in the vertical. The model physics includes the Grell cumulus parameterization scheme (Grell et al., 1994), the Graupel (reisner2) microphysical scheme, and the MRF planetary boundary layer (PBL) scheme. No cumulus parameterization is used in D02.

The global final (FNL) analysis data of the National Centers for Environmental Prediction (NCEP) with a $1°\times1°$ horizontal resolution are used as the model initial and boundary conditions. At the initial time of simulation, a bogus scheme (Low-Nam and Davis, 2001) is used to adjust the initial location, scale, and intensity of the typhoon in the initial field. The simulation is initialized at 2000 BT 31 September 2005, integrated for 72 h, and the output is produced every 1 h.

2.2 Verification of the model results

2.2.1 Track

Typhoon Talim moved northwestward consistently after it made landfall. Figure 1 shows the simulated and observed tracks of Talim when it was near Fujian Province. The mean track forecasting error is about 50 km. The simulated typhoon moved mainly in the northwest direction, which is consistent with the observation. However, there is a little northward deviation between simulation and observation from 2000 BT 1 to 0800 BT 2 September 2005.

2.2.2 Weather patterns

It can be seen from the 500-hPa geopotential height field of the NCEP reanalysis data (Fig. 2a) that there was a subtropical high to the northeast of Talim and a land high to its northwest at 1400 BT 1 September. To the north of 40°N, there was a trough. The two highs were connected at 0800 BT 2 September (Fig. 2b). Then, the geopotential height of the Talim center was obviously increased, and its intensity was weakened. At 0200 BT 3 September, the subtropical high and land high were disconnected again, moving to the east and west respectively (figure omitted). The northern trough moved southward to near 35°N. Talim was affected more by the trough, and the cyclonic circulation was further weakened. At about 0800 BT 4 September, the remnant cyclonic circulation of Talim disappeared.

Consistent with the observation, the simulated 500-hPa geopotential height field also displayed a subtropical high in the east of Talim, a land high in the west, and a trough in the north at 1400 BT 1 September (Fig. 2c). The subtropical high and the land high moved westward and eastward, respectively. By 0400 BT 2 September, they were completely connected (Fig. 2d), which was about 1 h earlier than the observation. Then, they separated soon and Talim was affected by the southeasterlies to the south of the subtropical high, which steered the typhoon to move more northward than the observation. On September 2, Talim moved into Jiangxi and then weakened. At 0200 BT 3 September, the remnant depression circulation was located over the adjoining areas of Jiangxi, Hunan, Hubei, and Anhui, very close to the observation.

2.2.3 Precipitation characteristics

The landfall of Talim was accompanied by very heavy rainfall. It is found from the conventional surface rain gauge data that when it was around the landing time of Talim in Fujian, the 24-h rainfall from 0800 BT 1 to 0800 BT 2 September was mainly concentrated in Fujian Province and south of Zhejiang Province, with the most intensive precipitation occurring in the adjoining area of Fujian and Zhejiang provinces to the right of the Talim track (Fig. 3a). The Fuding station had the largest daily precipitaiton of 236.8 mm. From 0800 BT 2 to 0800 BT 3 September, the main rainfall area moved northward to the mountain areas of Lushan and Dabieshan, which was 300–500 km away from the Talim center (Fig. 3b). The two maximum daily rainfall centers lay over the Lushan station in Jiangxi and Huoshan station near Dabieshan of Anhui, with daily rainfall reaching 494.6 and 254.8 mm, respectively (Fig. 3b). From 0800 BT 3 to 0800 BT 4 September, the heavy rainfall still maintained in Lushan and Dabieshan areas (figure omitted). Lushan and Huoshan stations recorded the largest rainfall, and the maximum total rainfall at Lushan station in Jiangxi exceeded 940 mm.

Based on the observed rainfall distribution, we define the heavy rainfall area I (Fig. 3a), which was located within a radius of 300 km from the typhoon center, or in the adjoining areas of Zhejiang and Fujian

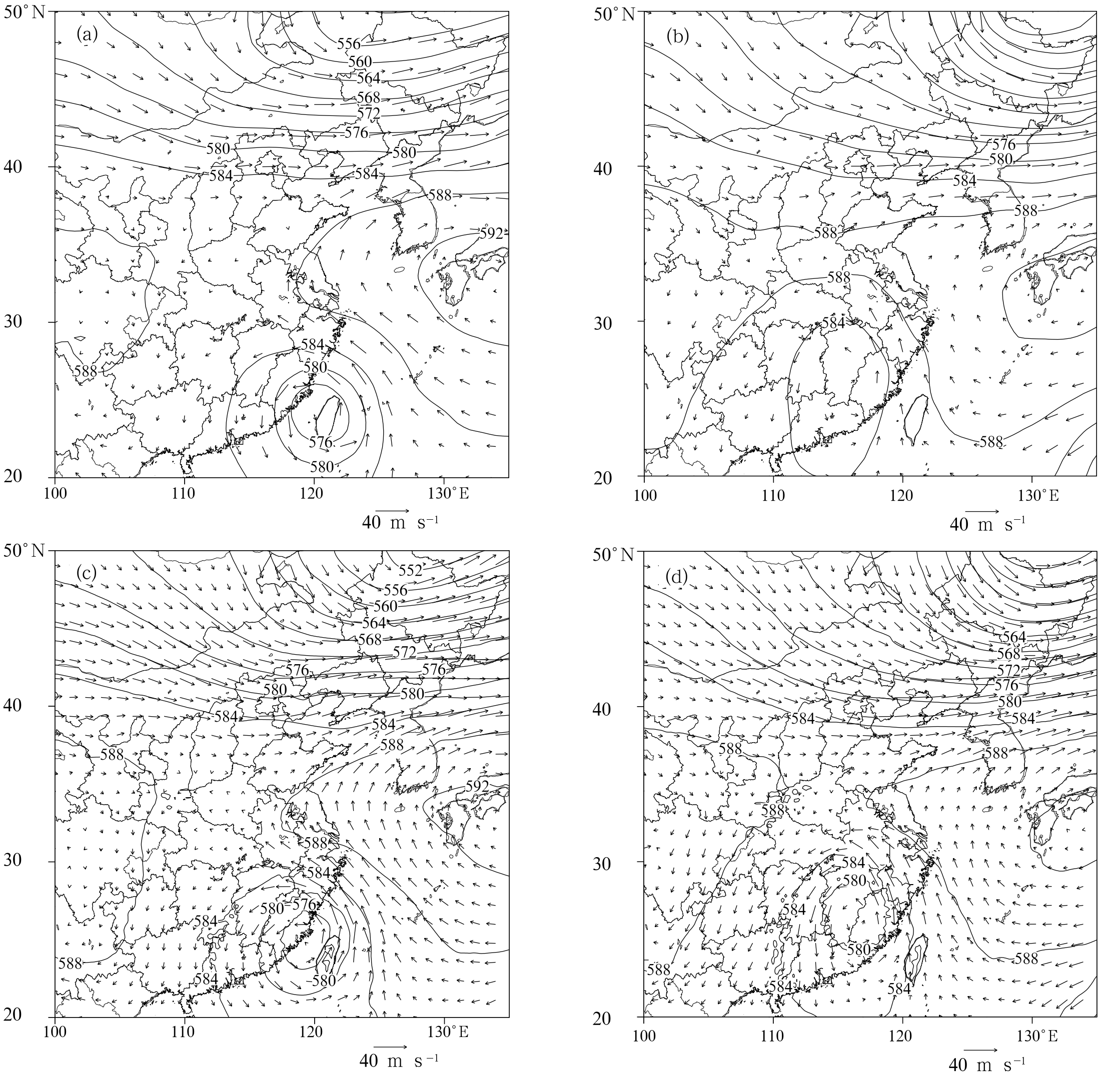

Fig. 2. 500-hPa geopotental height (contour) and wind vectors from (a, b) the NCEP reanalysis and (c, d) the MM5 simulation at 1400 BT 1 (a, c) and 0800 BT 2 (b, d) September 2005.

to the right of the typhoon track when Talim had just made landfall. When Talim moved further inland, though its main body weakened, there existed the heavy rainfall area II (Fig. 3b) in Lushan and Dabieshan areas, which was 300–500 km away from the typhoon center.

The simulated rainfall patterns are shown in Figs. 3c, d. From 0800 BT 1 to 0800 BT 2 September, the most intensive rainfall in the simulation was also located in the adjoining areas of Fujian and Zhejiang provinces, with the maximum rainfall amount exceeding 300 mm (Fig. 3c). From 0800 BT 2 to 0800 BT 3 September, the main rainfall area moved to the area near Lushan and Dabieshan (Fig. 3d). Thus, the simulated rainfall pattern was quite comparable to the observed one. For example, the simulated 24-h rainfall at Lushan station in Jiangxi was 340 mm, only a little lower than the observation. The simulated 24-h rainfall at Huoshan station in Anhui was about 300 mm, while the observation was 254.8 mm.

In short, although the simulated results are a little different from the observations, they could still well reflect the real weather process. In the next section, we will analyze the relation between H_2 and the rainfall from Typhoon Talim by using the simulated results, and explore the physical mechanisms that have

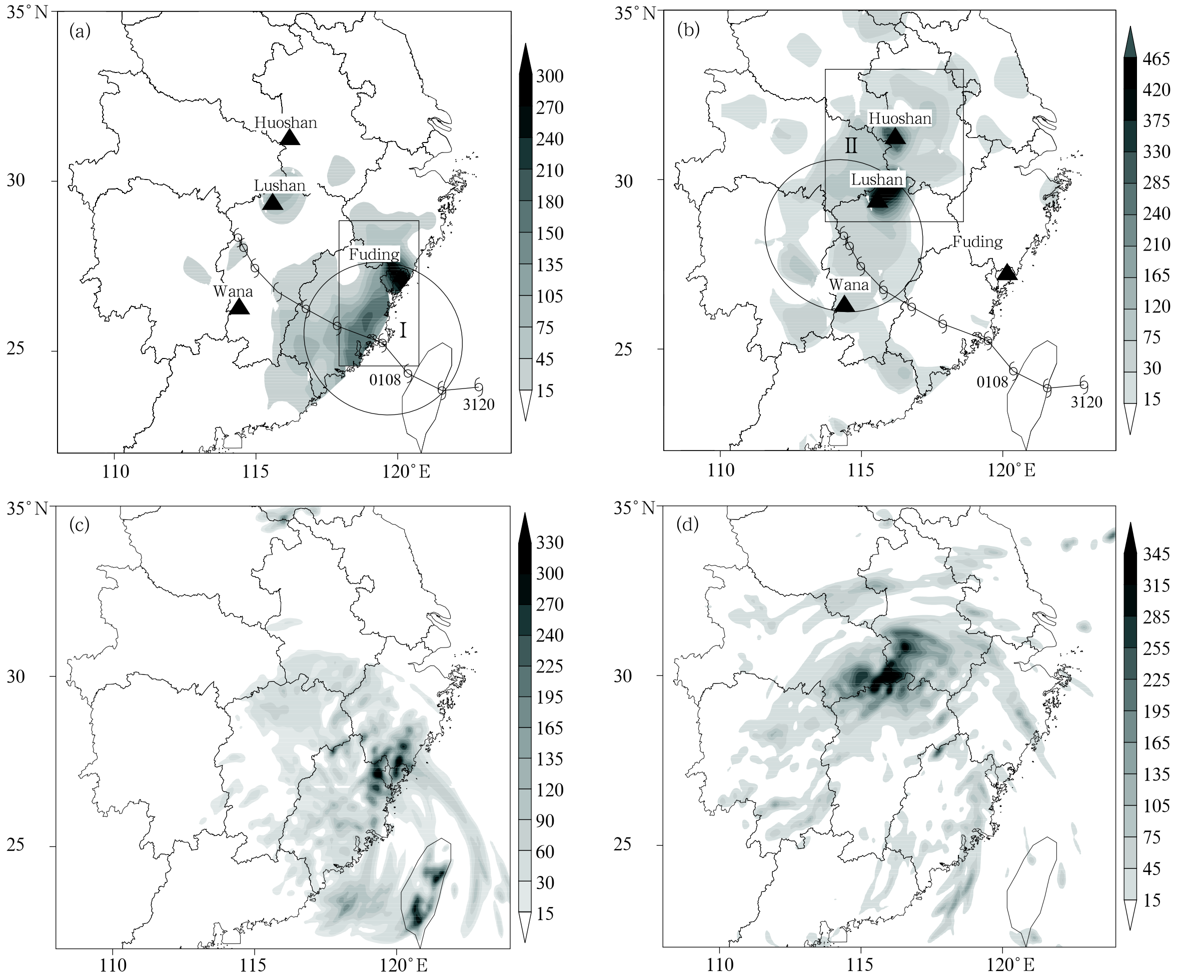

Fig. 3. Observed (a) and simulated (c) 24-h total rainfall (mm) from 0800 BT 1 to 0800 BT 2 September; observed (b) and simulated (d) 24-h total rainfall from 0000 BT 2 to 0800 BT 3 September. The rectangular frame and the square in (a) and (b) represent heavy rainfall areas I and II, respectively; the circles represent domains within a radius of 300 km from the center of Talim at 1400 BT 1 and 1400 BT 3 September, respectively.

sustained the rainfall.

3. Relation between H_2 and rainfall

The second type thermal helicity H_2 is defined (Yu and Wang, 2005; Du et al., 2007) as follows:

$$H_2 = -u\frac{\partial v}{\partial z} + v\frac{\partial u}{\partial z}. \tag{1}$$

It describes the interaction between the horizontal vorticity tube formed by vertical shear of horizontal wind and the wind vectors of weather systems. Different from helicity, H_2 mainly reflects the effect of the vertical wind shear on the secondary vertical circulation.

If the vertical shear of horizontal wind satisfies the thermal wind approximation, that is

$$\begin{aligned} \frac{\partial u_g}{\partial z} &= -\frac{g}{f}\frac{\partial}{\partial y}\ln T, \\ \frac{\partial v_g}{\partial z} &= \frac{g}{f}\frac{\partial}{\partial x}\ln T, \end{aligned} \tag{2}$$

then it can be deduced from Eqs. (1) and (2) that H_2 could reflect the interaction between the vertical wind shear caused by the inhomogeneous horizontal temperature distribution and the wind vectors, which is equivalent to the effect of horizontal temperature advection.

3.1 Diagnosis of the station rainfall

Fuding and Lushan stations received heavy rainfall when Talim just made landfall and moved further inland. First of all, rainfall variations at the two stations are diagnosed by examining H_2 and the helicity H_e, and then the results from the two methods are compared. To make the calculated values more representative, H_2 and H_e are averaged over the area with a radius of 50 km from the stations and are then compared with the hourly rainfall at the stations.

Figure 4a shows the diagnosis of the rainfall at Fuding station with H_2 and H_e. The most intensive rainfall occurred during 0800–2200 BT 1 September with three rainfall intensity peaks at 1400, 1800, and 2100 BT. H_2 results are consistent with the rainfall observation, indicating that H_2 can diagnose the rainfall variation at Fuding station (there is a 1-h time lag for the last peak). Meanwhile, H_e can also reflect the rainfall variation.

On the other hand, for the rainfall variation at Lushan station (Fig. 4b), H_2 at 850 hPa matches better with rainfall than H_e. The H_2 values also exhibit peaks that correspond to the four rainfall peaks at 0800, 1700, 2300 BT 2, and 0700 BT 3 September. However, the first and second rainfall peaks reflected by H_e were 2–4 h later than the observations, and the third and fourth rainfall peaks did not appear. The phase of H_e was also greatly different from that of the rainfall.

To further assess the ability of H_2 in indicating station rainfall, the correlation coefficient between H_2 and hourly rainfall at all stations is analyzed (Fig. 5). It is found that H_2 had a higher correlation coefficient with hourly rainfall than H_e, with a maximum value of 0.68, when Talim moved further inland (after 2000 BT 1 September). Moreover, the averaged correlation coefficients at 48 h were 0.47 and 0.40 respectively for H_2 and H_e, which are significant at the significance level of 0.05. Thus, H_2 could better reflect the inland rainfall variation of Talim. However, when Talim was about to make landfall (at about 2000 BT 1 September), the correlation coefficient between H_2 and rainfall was obviously lower than that between H_e and rainfall, so H_e showed some superiority during this stage. Therefore, H_2 had different abilities for predicting rainfall at different landfalling stages of a typhoon and the reason will be discussed in Section 4.

Further analyses of the correlation between the physical quantities at 1–5 h ahead of the rainfall and

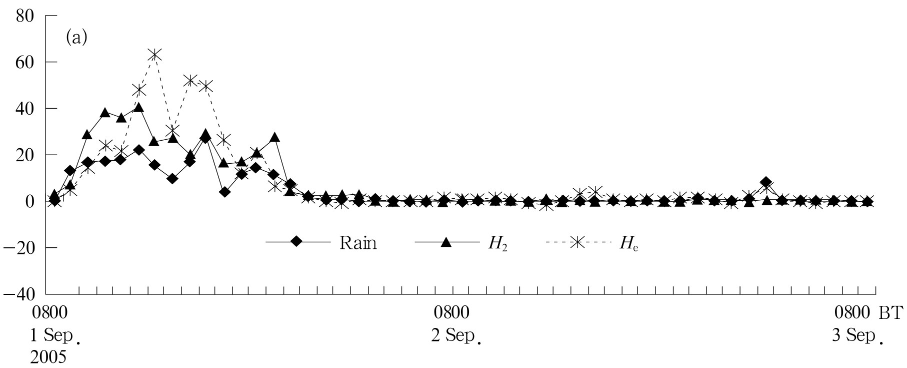

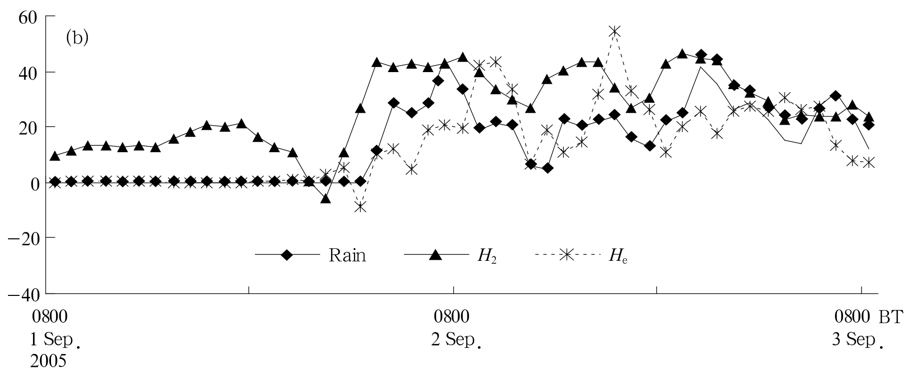

Fig. 4. Simulated hourly rainfall (mm), H_2 (0.3×10^{-2} m s^{-2}), and H_e (0.2×10^{-5} m s^{-2}) at (a) Fuding and (b) Lushan stations.

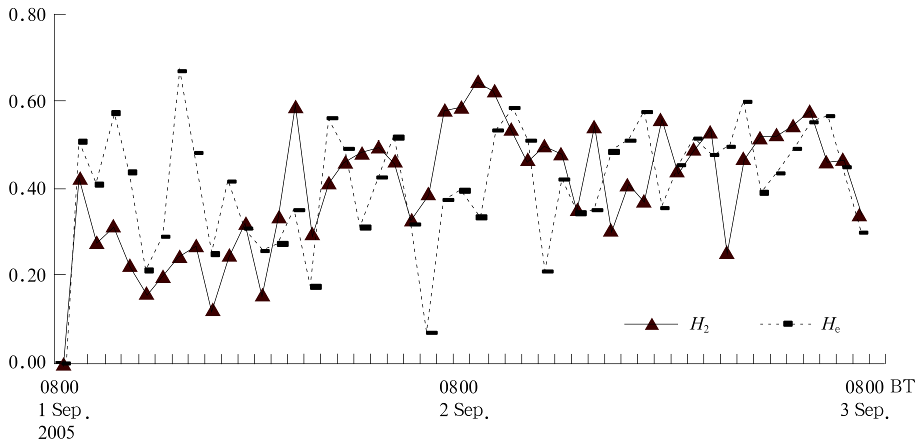

Fig. 5. Hourly variations of the correlation coeffecients between the simulated rainfall and H_2/H_e. The solid line is for H_2 and the dashed line is for H_e.

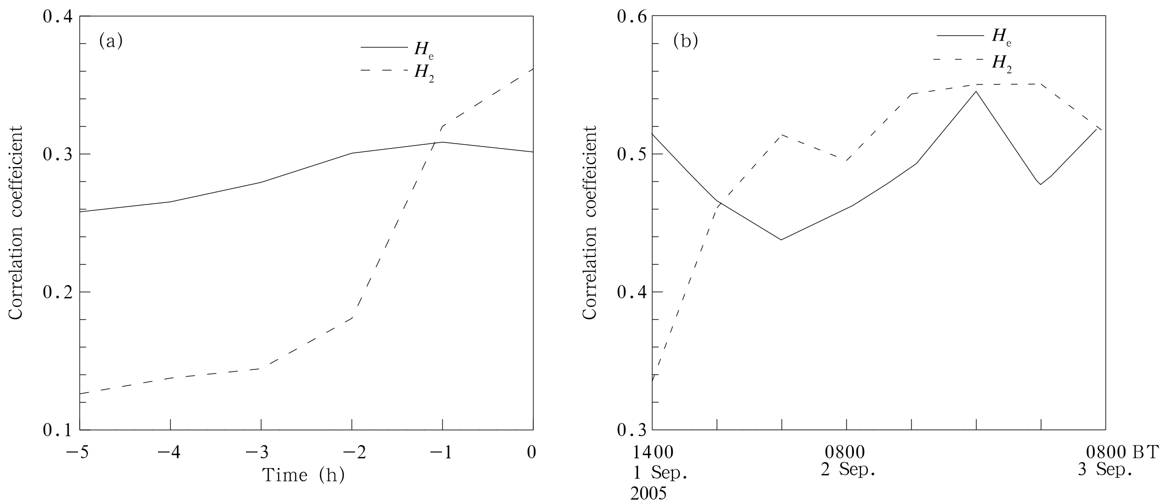

Fig. 6. (a) Correlation coefficients between rainfall and H_2/H_e at 5, 4, 3, 2, 1, and 0 h before the rainfall (shown by –5, –4, –3, –2, –1, and 0 on x-axis). (b) Correlation coefficients between rainfall and 6-h averaged H_2/H_e.

the station rainfall are made (Fig. 6a). It is found that the correlation coeficients between H_2/H_e and rainfall reached the same value at 1 h, but the correlation coefficient for H_2 was higher than that for H_e after that. This shows a better ability of H_2 to forecast rainfall amplification.

3.2 Diagnosis of the rainfall distribution

To assess the ability of H_2 in diagnosing the rainfall distribution during different landfalling stages and to compare with that of H_e, the variables H_2, H_e, and rainfall are averaged every 6 h.

During the 6 h before the Talim landfall, rainfall mainly occurred in the adjoining area of Zhejiang and Fujian provinces. The high value areas of H_2 coincided with the rain areas, but with a larger spatial coverage (Fig. 7a). On the other hand, the high value areas of H_e were a little scattered though they basically matched the rain areas (Fig. 7b). With the northwestward moving of the typhoon, the high value centers of H_2 moved northward. After Talim made landfall 24 h later, the H_2 centers well reflected the heavy rainfall area II (Fig. 8). The high value areas of H_e also maintained near the mountain areas of Lushan and Dabieshan. Though they matched the rainfall areas to some extent, their spatial coverage was much

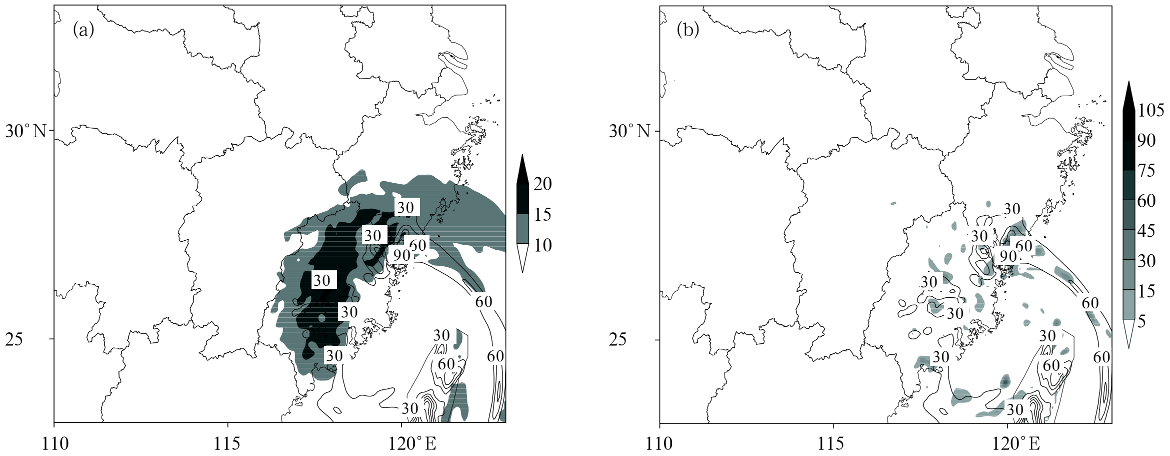

Fig. 7. 6-h averaged (a) H_2 (1×10^{-2} m s^{-2}) and (b) H_e (1×10^{-5} m s^{-2}) at 850 hPa (shaded) and 6-h averaged simulated rainfall (coutour number) before the Talim landfall from 0800 BT to 1400 BT 1 September.

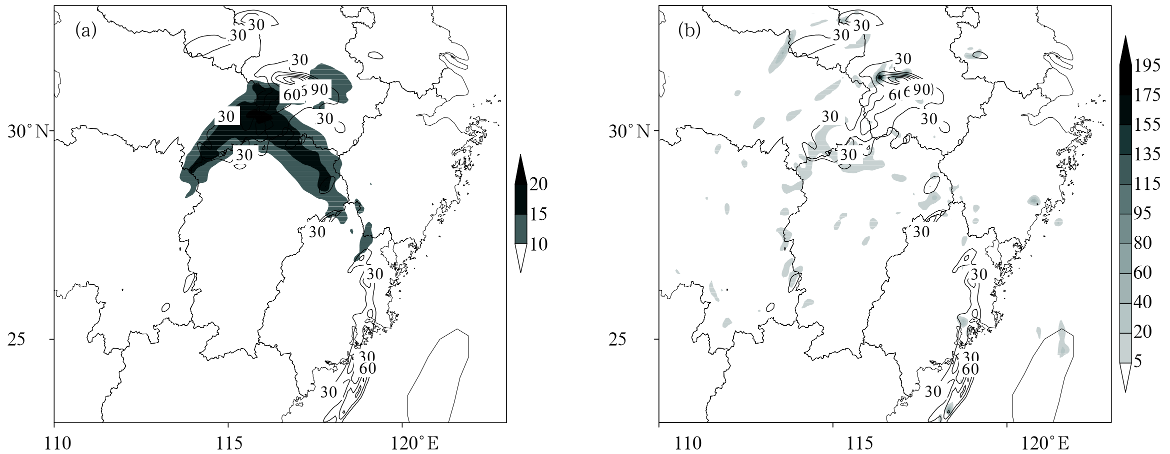

Fig. 8. As in Fig. 7, but for the 6 h after the Talim landfall from 1400 to 2000 BT 2 September.

smaller (Fig. 8b).

The correlation coefficients between rainfall and H_2/H_e averaged over each 6 h are shown in Fig. 6. It is found that before 2000 BT 1 September, the correlation coefficients between H_e and rainfall were larger than 0.5, higher than those between H_2 and rainfall. But after 2000 BT 1 September, the correlation coefficients between H_2 and rainfall increased and were higher than that of H_e. Therefore, although H_2 had a strong ability in diagnosing the station rainfall variation and rainfall distribution, it performed differently during different typhoon landfalling stages. In the next section, we will investigate the dynamic and thermal mechanisms of the heavy rainfall from Talim, and analyze the possible reasons for the differences of the diagnostic ability of H_2 during different typhoon landfalling stages.

4. Dynamic and thermal mechanisms of the heavy rainfall

During the landfall of Talim, the main rain area I was located in the adjoining area of Zhejiang and Fujian provinces (Fig. 3a). The main rain area gradually moved to the areas of Lushan and Dabieshan (rain area II) after Talim made landfall (Fig. 3b). In this section, we will analyze the reasons for the occurrences of rainfall in areas I and II.

4.1 Rainfall in area I

Heavy rain processes from a landfalling typhoon could be caused by many reasons: (1) they result from the main body of a typhoon; (2) the air convergencec caused by the influence of underlying surface on a landfalling typhoon produces or intensifies rainfall; (3) interactions between typhoon and baroclinic weather systems in mid and high latitudes results in the rainfall. Figures 9c and 9d illustrate the distributions of averaged lower-level vertical wind velocity and vorticity in rain area I. It is found that the upward motion was salient during the heavy rain from 0800 BT to 2000 BT 1 September, but the vertical wind velocity peak fell behind the rainfall peak (Fig. 9c). For relative vorticity, the increase of its values corresponded to the intensification of rainfalls, while the decrease of its values corresponded to the reduction of rainfalls (Fig. 9d). From the definition of H_e, the high correlation between H_e and rainfall in this stage was mainly associated with the high correlation between the relative vorticity and rainfall. But the relative vorticity mainly reflects the horizontal circulation characteristic of typhoons, and the main rain area I near Fujian and Zhejiang provinces was located within the radius of 300 km from the typhoon center. Therefore, the heavy rainfall in this area was mainly related to the main body of the typhoon characterized by an asymmetric structure.

Further analyses are made on the temperature advection at 925 hPa, and divergence at 200 and 925 hPa. It is found that the positive temperature advection at 925 hPa had a small variation during the heavy rain

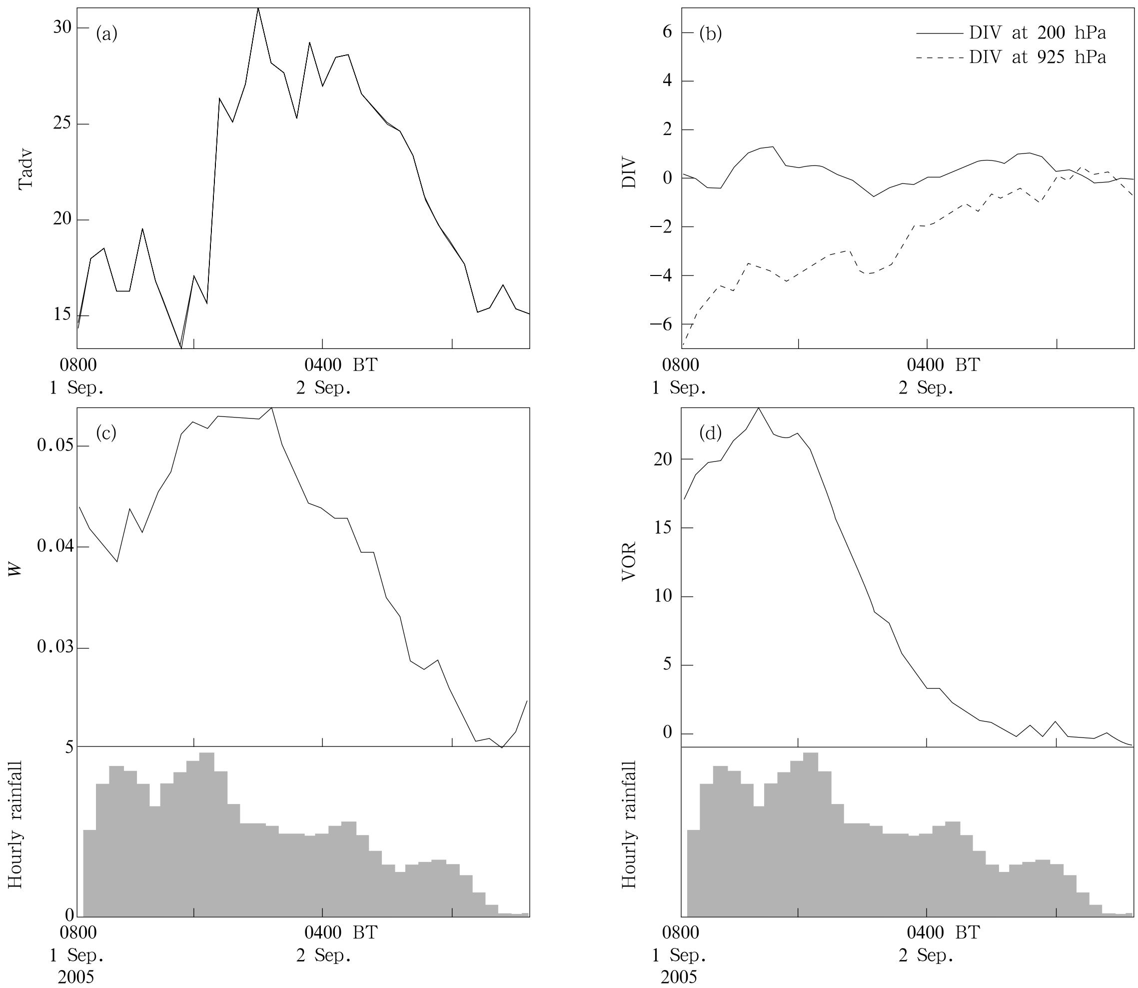

Fig. 9. Area-averaged (a) temperature advection (Tadv; 1×10^{-5} K s^{-1}) at 925 hPa, (b) divergence (DIV; 1×10^{-5} s^{-1}) at 200 and 925 hPa, (c) vertical velocity (W; m s^{-1}), and (d) relative vorticity (VOR; 1×10^{-5} s^{-1}) in the rain area I. The shaded bars in (c) and (d) denote the area-averaged hourly rainfall (mm).

period before 2000 BT 1 September, but it increased since the rain began to decrease after 2000 BT 1 September (Fig. 9a). The 200-hPa divergence values maintained around 1×10^{-5} s^{-1}, showing the weak upper-level divergence (Fig. 9b). Before landfall of Talim, the low-level air convergence was the strongest. With the typhoon approaching the main land, the 925-hPa negative divergence value increased gradually, i.e., the air convergence at low levels weakened. This is consistent with the geopotential height analysis in Fig. 2a, i.e., Talim was not obviously influenced by the baroclinic systems like the westerly trough at that time and the lower-level air convergence and upper-level air divergence were not strong then. Thus, the lower-level temperature advection and rainfall in area I were out of phase, and the upper-level air divergence was weak. It is discovered that the heavy rainfall was not connected with the interactions of the baroclinic systems in mid and high latitudes. In addition, the differences in underlying surface conditions would generally generate or intensify the rainfall when the outer circulation of a typhoon arrives at land. But in this case, the low-level air convergence had reached the greatest value before the rainfall peak occurred in area I. This indicates that terrains of Zhejiang and Fujian provinces and the differences in land-sea contrast were not the main reasons for the continuous heavy rainfall in area I.

4.2 Rainfall in area II

4.2.1 Temperature advection and divergence

The low-level temperature advection, upper-level divergence, and rainfall in the heavy rain area II are analysed here. The rain began at 0000 BT 2 September and was intensified gradually (Fig. 10). A peak of the rainfall showed up at 1900 BT 2 September. With the increase of the rain intensity, positive temperature advection at 925-hPa appeared and turned larger gradually. The maximum temperature advection took place at 1800 BT 2 September (Fig. 10a). The 200-hPa divergence was always positive, while the 925-hPa divergence was negative, and their absolute values were quickly increasing from 0000 BT 2 September, displaying a pronounced pattern of lower-level air convergence and upper-level air divergence (Fig. 10b).

Figure 11 shows that the typhoon center was located beyond a distance of three latitude degrees from the heavy rain center. At the beginning of the rain at 0400 BT 2 September, there was a notable upper-level jet located northeast of the typhoon at 200 hPa.

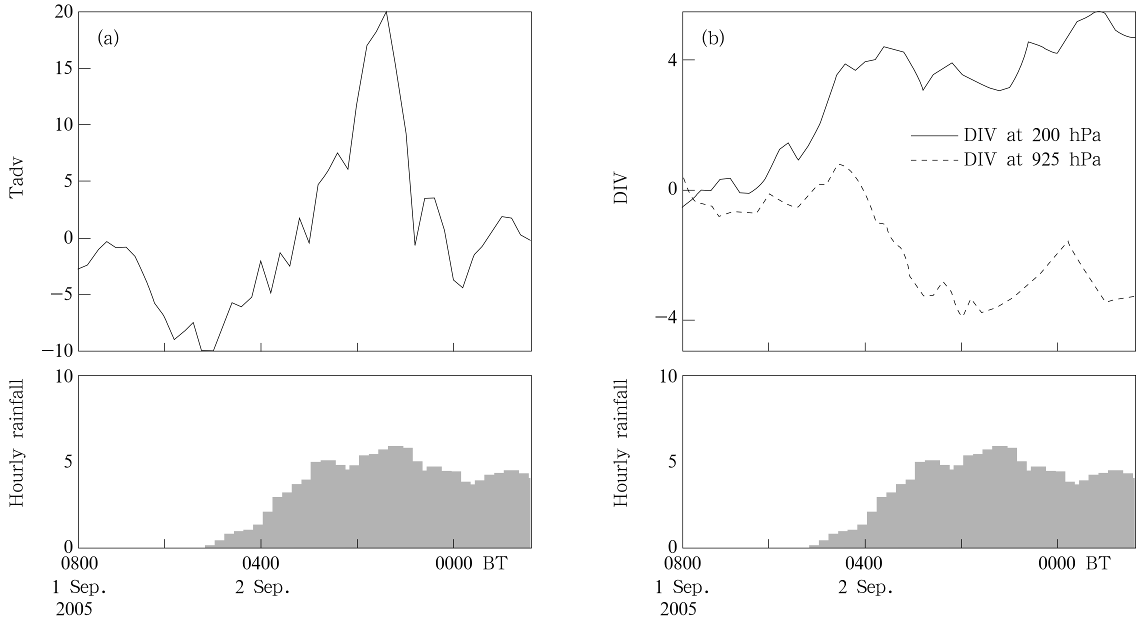

Fig. 10. The lower pannels of (a) and (b) show the area-averaged hourly rainfall (mm, shaded). The upper pannel of (a) shows the temperature advection (Tadv; 1×10^{-5} K s^{-1}) at 925 hPa and the upper pannel of (b) shows the area-averaged divergence (DIV; 1×10^{-5} s^{-1}) at 925 and 200 hPa in the rain area II.

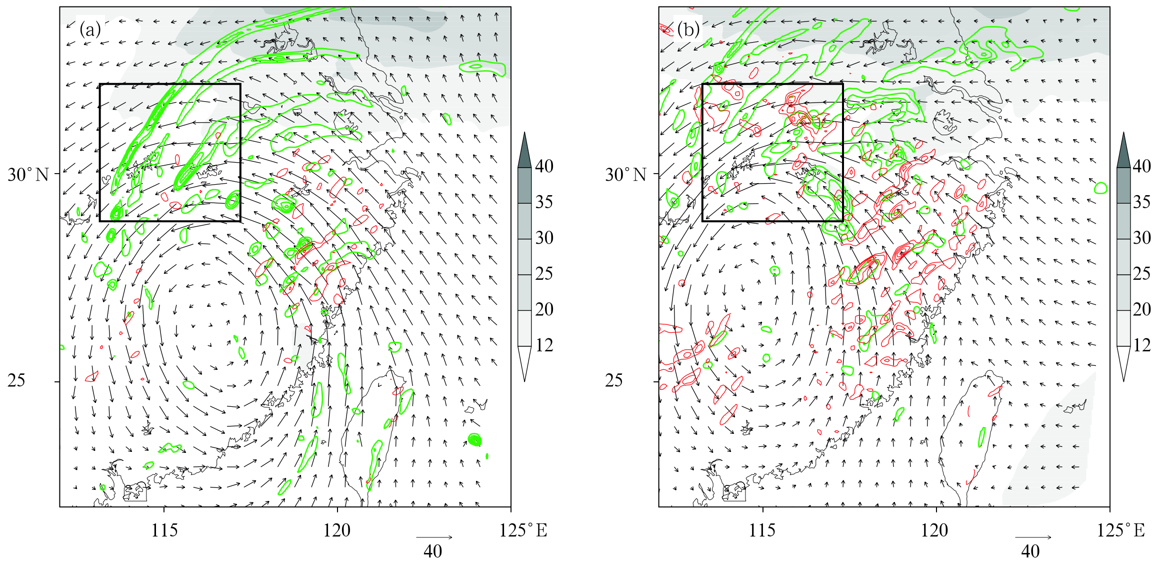

Fig. 11. The 850-hPa wind vector field, 850-hPa positive temperature advection (red contours), 200-hPa jet areas (shaded; $\geqslant$ 12 m s^{-1}), and 200-hPa positive divergence areas (green contours) at (a) 0400 BT and (b) 1900 BT 2 September 2005.

Under the effects of outflow of the upper-level jet, a positive divergence area was right in the entrance of the jet, which was just above the heavy rain area. The 925-hPa positive temperature advection existed but was weak. Later, the upper-level positive divergence and lower-level positive temperature advection were gradually turning larger, followed with the rainfall intensification (Fig. 10). Until 1900 BT 2 September, the rainfall became the heaviest, and the upper-level jet still maintained in the north and became a little stronger. There were strong positive lower-level temperature advection and upper-level divergence (Fig. 11b). Furthermore, after Talim made landfall, no obvious positive lower-level temperature advection and upper-level divergence appeared within the area of a radius of 200 km from the Talim center (Fig. 11). Therefore, the westerly trough had no obvious effects on the maintainance of Talim intensity after its landfall. Then, Talim dissipated gradually without adequate support for its maintenance.

4.2.2 Vertical wind shear

Figure 10 shows that with the continuous rainfall after 1800 BT 2 September, the positive 925-hPa temperature advection began to decrease quickly, while the positive 200-hPa divergence was keeping strong, suggesting that the thermal effects of lower-level positive temperature advection were not related to the maintenance of the rainfall after 1800 BT 2 September. In fact, the wind field played an important role in activities of tropical cyclones. According to the theory of thermal wind, the horizontally-uneven thermal distribution can cause vertical wind shear. Meanwhile, the dynamical forcing of underlying surface and meso-micro scale terrains can also induce large-scale environmental wind changes, producing the vertical wind shear.

Figure 12 demonstrates the variation of zonal (U) and meridional (V) winds averaged in the area with a radius of 500 km from the Talim center during its landfall. The 200-hPa U and V (U_{200} and V_{200}) were stably increasing and U_{200} was always positive and greater than V_{200} after the typhoon landfall. This shows that the averaged upper-level winds were from northwest with a dominant westerly component. But the lower-level wind components (U_{850} and V_{850}) were different, with V_{850} increasing while U_{850} decreasing. Thus, combined with the analyses of the weather pattern in Fig. 2, these differences between lower- and upper-level wind fields indicate that Talim was co-affected by the northwest wind of the subtropical high and the southwest wind in front of the upper-level trough, and the effects of the upper-level trough became more and

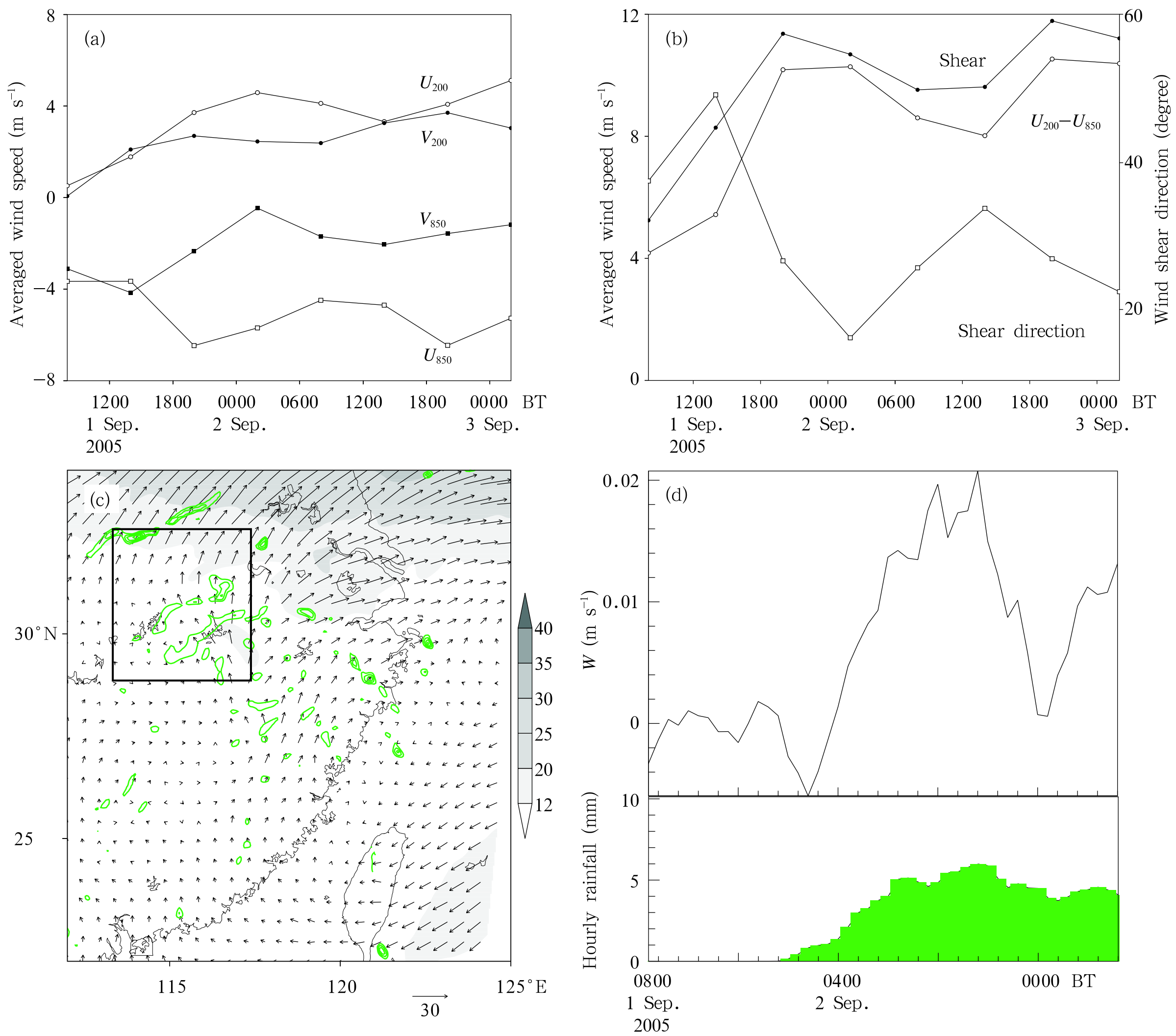

Fig. 12. (a) Variations of the zonal and meridional wind components averaged within the area with a radius of 500 km from the typhoon center at 850 and 200 hPa (U_{850}, V_{850}, U_{200}, and V_{200}). (b) Variations of the vertical wind shear magnitude, shear direction, and zonal wind differences between upper and lower levels (U_{200}–U_{850}). (c) 200-hPa upper-level jet (shaded, $\geqslant$ 12 m s^{-1}), wind vectors, and 850-hPa positive vertical wind (green contours). (d) Variations of the averaged vertical wind speed (W, curve, m s^{-1}) and hourly rainfall (shaded) for area II.

more significant.

Figure 12b shows the variation of vertical wind shear at 850 and 200 hPa. During the Talim landfall, the vertical wind shear direction angle was decreasing. The shear direction changed from northeast (52°) to east (19°). Since Talim was moving northwestward, the shear direction was always to the southeast of Lushan and Dabieshan. Thus, Lushan and Dabieshan were located on the left side of the down shear, and U_{200}–V_{850} was the main contributor to the vertical wind shear. Near the landing time, the magnitude of the vertical wind shear was only 5 m s^{-1}, but it gradually increased to 11–12 m s^{-1} with Talim movi-ng further inland.

In summary, for the rain area II, Talim was co-affected by the lower-level northwest wind of the subtropical high and the upper-level outflow of the westerly trough when it moved further inland, and the vertical wind shear effects on the typhoon were gradually increasing. Lushan and Dabieshan were located right on the left side of the vertical wind shear, and thus the heavy rainfall in area II was induced. However, the positive lower-level temperature advection decreased quickly after 1900 BT 2 September, and the heavy rainfall maintained in the mountain areas. Whether this was connected with the meso-micro scale topographic effecct is still unknown. On the other hand, under the effects of the vertical wind shear, the mountain areas of Lushan and Dabieshan were dominated by an easterly upper-level jet that was advantageous to divergence and secondary vertical circulation. Therefore, the convection was spawn over there and strong upward motion appeared (Fig. 12c). The averaged maximum vertical wind speed in area II corresponded to the rainfall peak (Fig. 12d). This is consistent with previous results that on the left side of down shear, the vertical circulation can easily be induced and the convection is developed (Willoughby et al., 1984; Marks et al., 1992; Franklin et al., 1993; Gamache et al., 1997; Corbosiero and Molinari, 2002; Black et al., 2002).

5. Conclusions

In this paper, we use the mesoscale model MM5 to simulate the landfalling process of Typhoon Talim. The simulated typhoon track, the weather pattern, and the rainfall process are basically consistent with the observations. Based on the simulation results, the relation of H_2 with the rainfall from the landfalling Talim is studied. The results show that H_2 was useful in diagnosing the heavy rainfall inland but it performed not so well when the typhoon just made landfall.

In particular, H_2 was highly correlated with rainfall at 1 h forecast lead time. During 1–5-h prediction lead time, H_2 had a higher correlation with rainfall than H_e, and thus it showed a better ability in forecasting rainfall intensification.

Further analyses found that when Talim was in the initial stage of landfall, the 850–200-hPa vertical wind shear around the Talim center was quite small (about 5 m s^{-1}). The highest rainfall was to the right of the Talim track and in the area with a radius of 300 km from the Talim center, and it had no obvious relation to the low-level temperature advection, low-level air convergence, and upper-level divergence. However, the low-level relative vorticity could reflect the rainfall change quite well, which was the main reason why H_e had a better performance than H_2 in prediction of rainfall during this period. But after Talim moved inland further, it was obviously affected by the trough in the north. The heavy rainfall over the Lushan and Dabieshan areas were closely associated with the increasing vertical wind shear, and therefore, H_2 showed its good ability to reflect rainfall variation and distribution during this stage.

REFERENCES

Black, M. L., J. F. Gamache, F. D. Marks, et al., 2002: Eastern Pacific hurricanes Jimena of 1991 and Olivia of 1994: The effect of vertical shear on structure and intensity. *Mon. Wea. Rev.*, **130**, 2291–2312.

Chen Lianshou, 1977: Reason analysis of heavy rainfall caused by landfalling typhoons. *Meteor. Mon.* **11**, 10–13. (in Chinese)

Cheung, K. W., Li-Rung Huang, and Cheng-Shang Lee, 2006: A tropical cyclone rainfall climatology-persistence model for the Taiwan area. Preprints, 27th Conference on Hurricanes and Tropical Meteorology, Amer. Meteor. Soc.

Corbosiero, K. L., and J. Molinari, 2002: The effects of vertical wind shear on the distribution of convection in tropical cyclones. *Mon. Wea. Rev.*, **130**, 2110–2123.

Du Xiaoling, Yu Zifeng, Lu Chongming, and Wang Yuan, 2007: A research on the mechanism for the Shanghai heavy rainfall event on 5–6 August 2001 caused by a tropical depression. *J. Nanjing University* (*Natural Sciences*), **43**(6), 621–633. (in Chinese)

Dudhia, J., G. Dave, Y. R. Guo, et al., 2001: PSU/NCAR Mesoscale Modeling System Tutorial Class Notes and User's Guide (MM5 Modeling System Version 3). Available online at http://www.mmm.ucar.edu/mm5/mm5v3/tutorial/teachyourself.html.

Franklin, J. L., S. J. Lord, S. E. Feuer, and F. D. Marks Jr., 1993: The kinematic structure of Hurricane Gloria (1985) determined from nested analyses of dropwindsonde and Doppler radar data. *Mon. Wea. Rev.*, **121**, 2433–2451.

Gamache, J. F., H. E. Willoughby, M. L. Black, and C. E. Samsury, 1997: Wind shear, sea surface temperature, and convection in hurricanes observed by airborne Doppler radar. Preprints, 22nd Conf. Hurricanes and Tropical Meteorology, Fort Collins, CO, Amer. Meteor. Soc., 121–122.

Gao, S., X. Wang, and Y. Zhou, 2004a: Generation of generalized moist potential vorticity in a frictionless and moist adiabatic flow. *Geophys. Res. Lett.*, **31**, L12113, doi: 10. 1029/2003GL019152.

——, F. Ping, X. Li, et al., 2004b: A convective vorticity vector associated with tropical convection: A two dimensional cloud-resolving modeling study. *J. Geophys. Res.*, **09**, D14106, doi: 10. 1029/2004JD004 807.

——, Y. Zhou, T. Lei, et al., 2005: Analyses of hot and humid weather in Beiing City in summer and its dynamical identification. *Sci. China (Ser. D)*, **48**(Suppl. II), 128–137.

Gao Shouting, 2007: *Dynamical Basics and Forecasting Methods of Atmospheric Mesoscale Motion.* China Meteorological Press, Beijing, 68–69. (in Chinese)

Grell, G. A., J. Dudhia and D. R. Stauffer, 1994: A Description of the Fifth–Generation Penn State/NCAR Mesoscale Model (MM5). NCAR Technical Note, NCAR/TN–398 +STR, 1–117.

Kidder, Stanley Q., Sheldon J. Kusselson, John A. Knaff, Ralph R. Ferraro, Robert J. Kuligowski, and Michael Turk, 2005: The tropical rainfall potential (TRaP) technique. Part I: Description and examples. *Wea. Forecasting*, **20**(4), 456–464.

Lei Xiaotu and Chen Lianshou, 2001: Tropical cyclone landfalling and its interaction with midlatitude circulation systems. *Acta Meteor. Sinica*, **59**(5), 602–615. (in Chinese)

Low-Nam, S., and C. Davis, 2001: Development of a tropical cyclone bogussing scheme for the MM5 system. Preprint, The 11th PSU/NCAR Mesoscale Model Users' Workshop, June 25–27, 2001, Boulder, Colorado, 130–134.

Marks, F. D. Jr., R. A. Houze Jr., and J. F. Gamache, 1992: Dual-aircraft investigation of the inner core of Hurricane Norbert. Part I: Kinematic structure. *J. Atmos. Sci.*, **49**, 919–942.

——, and L. K. Shay, 1998: Landfalling tropical cyclones: Forecast problems and associated research opportunities. *Bull. Amer. Meteor. Soc.*, **79**, 305–323.

Moffatt, H. K., 1969: On the knottedness of tangled vortex lines. *J. Fluid Mech.*, **35**, 117–128.

Niu Xuexin, Du Huiliang, and Liu Jianyong, 2005: The numerical simulation of rainfall and precipitation mechanism associated with Typhoon Sinlaku (0216). *Acta Meteor. Sinica*, **63**(1), 57–68. (in Chinese)

Pfost, R. L., 2000: Operational tropical cyclone quantitative precipitation forecasting. *Natl. Wea. Dig.*, **24**, 61–66.

Rappaport, E. N., 2000: Loss of life in the United States associated with recent Atlantic tropical cyclones. *Bull. Amer. Meteor. Soc.*, **81**, 2065–2073.

Willoughby, H. E., F. D. Marks Jr., and R. J. Feinberg, 1984: Stationary and moving convective bands in hurricanes. *J. Atmos. Sci.*, **41**, 3189–3211.

Yu Zifeng and Wang Yuan, 2005: Theoretic Research and Numerical Simulation of Landfalling Tropical Cyclone Heavy Rainfall. Master thesis, Nanjing University, Nanjing, 24–25. (in Chinese)

Zhao Yu, Cui Xiaopeng, and Wang Jianguo, 2009: A study on a heavy rainfall event triggered by inverted typhoon trough in Shandong Province. *Acta Meteor. Sinica*, **29**(4), 468–484.